Metrol. Meas. Syst., Vol. 32 (2025), No. 3
DOI: 10.24425/mms.2025.155805

METROLOGY AND MEASUREMENT SYSTEMS
Index 330930, ISSN 0860-8229
www.metrology.wat.edu.pl

MEASUREMENT OF THE SYNTHETIC VESSELS MECHANICAL PROPERTIES USING A MAN-MADE CIRCULATORY MODEL

Andrzej Polanczyk[1)], Aleksandra Piechota-Polanczyk[2)],Agnieszka W. Piastowska-Ciesielska[2)], Ihor Huk[3)], Christoph Neumayer[3)], Patricia Pia Wadowski[4)], Julia Balcer[5)], Michal Strzelecki[5)]

1) *The Faculty of Safety Engineering and Civil Protection, Fire University, 01-629 Warsaw, Poland* (✉ *andrzej.polanczyk@gmail.com*)
2) *Medical University of Lodz, Department of Cell Cultures and Genomic Analysis, 90-752 Lodz, Poland*
3) *Department of Surgery, Division of Vascular Surgery, Medical University of Vienna, Währinger Gürtel 18-20, 1090 Vienna, Austria*
4) *Division of Angiology, Department of Internal Medicine II, Medical University of Vienna, Währinger Gürtel 18-20, 1090 Vienna, Austria*
5) *Institute of Electronics, Lodz University of Technology, 93-590 Lodz, Poland*

Abstract

Ex-vivo vessel culture systems that simulate hemodynamic factors enable the measurement of flow and pressure conditions. However, limited efforts have been made to use *ex-vivo* vessel bioreactors to accurately replicate the hemodynamic factors influencing arterial wall behavior in an artificial setting. Therefore, the aim of this study was to examine the mechanical properties of different types of vessels (vascular grafts and human arteries) under various hemodynamic conditions using a specialized *ex vivo*. Additionally, the study compared different vascular grafts with human arteries. To achieve this, a Man-made Circulatory Model was designed and constructed to simulate vessel structure under varying flow conditions. The following vessel types were analyzed: ring-enforced ePTFE prostheses, Dacron prostheses, and iliac arteries. The initial conditions for the process were: pulsating flow at five frequencies (60, 75, 90, 105, and 120 1/min) and varying ejection volumes (EV) of homemade fluid per cycle (70, 85, 100, and 115 ml). Our findings suggest that pulsation frequency and ejection volume are key factors influencing the performance of these vascular prostheses. Additionally, we found that as pulsation frequency increases, the diameter dilation differences between iliac arteries and prostheses, as well as between the two types of prostheses, also change ($p<0.0001$). Specifically, the difference in dilation between the prostheses and the iliac arteries increases at higher frequencies, but the pattern of this increase varies between the prosthesis types, suggesting differences in their mechanical behavior under varying conditions of flow ($p<0.0001$). To sum up our approach may help guide clinical decisions on prosthesis selection.

Keywords: Iliac arteries, ring enforced ePTFE vascular prostheses, Dacron vascular prostheses, artificial system.

1. Introduction

Cardiovascular diseases (CVDs) continue to be a major global cause of illness and death, accounting for millions of fatalities annually [1, 2]. CVDs are among the leading causes of death in both Europe and the United States [3]. These diseases encompass a range of conditions affecting the heart and blood vessels, including coronary artery disease, heart failure, stroke, peripheral artery disease, and hypertension [4, 5]. Additionally, conditions such as obesity, diabetes, and high cholesterol significantly increase the risk of developing cardiovascular problems [6-8].

The systemic circulation includes veins, arteries, and blood vessels, all connected to the heart, which acts as a pump to circulate oxygen and nutrients throughout the body [9, 10]. The pulsatile flow of blood in the arterial system generates forces that repeatedly stretch the walls of the arteries, potentially causing damage, especially when pre-existing conditions such as atherosclerosis weaken the arterial walls [11]. As a result, both *in vivo* and *ex vivo* research is

Article history: received March 7, 2025; revised July 11, 2025; accepted August 4, 2025; available online September 17, 2025.

conducted to explore new strategies for protecting the human circulatory system [12]. However, *in vivo* studies, often performed on animal models, may not accurately reflect changes in the human body, and clinical studies may present ethical challenges. In contrast, *ex vivo* studies are less restrictive, as they can be performed on tissue samples or primary cells [13].

In blood flow research, image analysis plays a crucial role in examining raw data [14]. Various imaging processing algorithms for blood vessels detection may be applied [15, 16]. Most studies required manual identification of vessel edges [17]. Because manual blood vessel segmentation is slow and difficult, creating automatic methods is essential [18]. Automated blood vessel segmentation reduces manual effort and improves result objectivity [19]. Among other techniques, convolutional neural networks are used to measure vessel width with subpixel accuracy [20].

Recent advancements in medical research have highlighted the importance of early detection and prevention in managing cardiovascular diseases [21-23]. Biomarkers, imaging technologies, and genetic testing are increasingly used to identify high-risk individuals and monitor the disease's progression [24]. It creates the requirement to develop novel measurement systems for the identification and quantitative measurement of the parameters of elements within the human circulatory system.

Furthermore, recent biomedical research focuses on using biomaterials to recapitulate cells for therapeutic advancements and tissue regeneration [25]. Several *in vivo* models have been developed to investigate vascular biology, including *ex vivo* tissue culture systems, which serve as alternative models to *in vivo* animal studies and *in vitro* cell cultures for assessing vascular responses to biomechanical and biochemical factors [26]. *Ex vivo* vessel culture systems that simulate hemodynamic factors enable the study of flow and pressure conditions [27]. However, few efforts have been made to fully replicate the hemodynamic factors affecting arterial wall behavior in artificial settings. This study aims to measure the mechanical properties of various vessels (vascular grafts and human arteries) under different hemodynamic conditions using a specialized, computer-controlled vessel reactor. A dedicated system, the Man-made Circulatory Model, was designed and implemented for this purpose. It enables the measurement of vessel spatial deformation, which is crucial for assessing the mechanical behavior of vessels. The obtained measurement results were subjected to rigorous statistical analysis.

This paper is structured as follows: Section 2, 'Materials and Methods,' details the self-made apparatus, analyzed materials, and boundary conditions. Section 3, 'Results,' outlines the experimental findings. In Section 4, 'Discussion,' the results are thoroughly analyzed. Lastly, Section 5, 'Conclusions,' provides a summary of the key findings.

2. Material and Methods

The analysis of vessel mechanical behavior required simulating real hemodynamic conditions, both physiological and pathological. The *Man-made Circulatory Model* (MmCM) was designed to simulate vessel structures under varying flow conditions. The study focused on two groups of vessels: iliac arteries and synthetic prostheses (ring-enforced ePTFE, Dacron). We performed multiple analyses, each time using material from 10 patients and three technical repetition of each conditions. All vessels had a length of 100 mm and diameters of 0.1 mm (prostheses) and 0.5 mm (iliac arteries). Iliac arteries were sourced from ten male organ donors (aged 52 ± 10 years) treated at the Medical University of *Vienna* (2016-2017) and preserved in PBS solution. The study was approved by the local IRB (2069/2012).

The primary component of the MmCM was a transparent rectangular container (the vessel reactor) with thermal insulation designed to maintain a constant temperature. The vessels being analyzed were supplied with a homemade fluid that mimicked blood, composed of 60% distilled water and 40% glycerol, kept at a constant temperature of 37°C [28]. Pulsatile flow was

generated by a custom-built artificial heart, which controlled parameters such as ejection pressure, ejection volume, and pulsation frequency. The initial conditions for the process were set as follows: pulsatile flow with five different *pulsation frequencies* (PF): 60, 75, 90, 105, and 120 cycles per minute and varying *ejection volumes* (EV) of homemade fluid per cycle, specifically 70, 85, 100, and 115 ml. To ensure realistic inlet conditions for the vessels, the artificial heart was supplied with blood hemodynamic parameters as described in previous works [29, 30]. Additionally, to replicate the pressure exerted on the vessel's outer wall, similar to conditions in the human body, the transparent container was filled with distilled water at a constant temperature of 37°C. A *Custom-Designed Control and Data Acquisition* (CDCDA) system was created using LabView 2011 software (National Instruments, USA) to manage the artificial heart, temperature regulation, and a set of nine cameras. The cameras were mounted on an aluminum circular frame, parallel to the floor, enabling horizontal movement. To improve the accuracy of visual data capture, the cameras were adjustable in 10-degree increments within a 40-degree range. The SCADA system was integrated with a portable workstation, the Dell Precision M6400, equipped with a four-core Intel CPU (2.4GHz), 4GB of RAM (1333MHz), and a 500GB SSD hard drive.

To reconstruct the actual flow, two crucial parameters were considered: the frequently of pulsation and different ejection volumes. The analysis of the vessel's mechanical behavior concentrated on its capacity for spatial deformation. Two parameters were examined: the *diameter dilatation DD* (1) and the *wall displacement* (WD) (2).

$$DD = Ddynamic(x, y, z) - Dstatic(x, y, z) \tag{1}$$

where: *DD* – dilation of the vessel's diameter, [mm]; *Dstatic*(*x*, *y*, *z*) – vessel diameter measured under static conditions, [mm]; *Ddynamic*(*x*, *y*, *z*) – maximum vessel diameter measured under dynamic conditions, [mm].

$$WD = Wdynamic(xp', yp', zp') - Wstatic(xp, yp, zp) \tag{2}$$

where: WD – displacement of the vessel's wall, [mm]; *Wstatic*(*xp*, *yp*, *zp*) – spatial configuration of the vessel's wall relative to its central axis under static conditions; *xp*, *yp*, *zp* – spatial coordinates of a tracked point *p* located on the vessel's surface, [mm]; *Wdynamic*(*xp'*, *yp'*, *zp'*) – spatial configuration of the vessel's wall relative to its central axis under dynamic conditions; *xp'*, *yp'*, *zp'* – spatial coordinates of a tracked point *p* located on the vessel's surface, [mm].

Both parameters enabled the characterization of the spatial configuration of each analyzed vessel under varying hemodynamic conditions. DD reflected the vessel's circumferential behavior, while WD described its deviation from the central axis. Medical data was used to verify the MmCM results. The *2D-speckle-tracking technique* (2DSTT) was utilized to evaluate changes in the diameter across three patient groups: ten with ring-enforced ePTFE vascular prostheses, ten with Dacron vascular prostheses, and ten without either type of vascular prostheses (represented by iliac arteries). For standardization, measurements were taken under the following conditions: PF of 75 1/min and 90 1/min, with an EV of 70 ml. Finally, the MmCM results were compared to the medical data obtained under the same hemodynamic conditions.

Statistical analysis was carried out using Statistica 12.0 (USA). The data are presented as mean ± *standard error* (S.E.) and, when applicable, as median with interquartile range. The Bland-Altman method was applied to evaluate the agreement between 2DSTT and MmCM data, along with Spearman's correlation analysis. Comparisons between groups were performed using the Wilcoxon Rank-Sum test or paired Student's *t*-test, based on normality and variance assessments. A *p*-value of less than 0.05 was considered statistically significant, unless indicated otherwise.

3. Results

The study explored the flexibility of artificial and real vessels made from materials such as ePTFE, Dacron and human tissue. Initially, the relationship between *DD* and *WD* as functions of EV and PF was analyzed.

3.1. Diameter dilatation

The analysis of circumferential stresses revealed that the iliac arteries and Dacron vascular prostheses experienced the highest DD. An increase in EV and PF led to a rise in DD (from 0.83±0.019 mm to 1.49±0.008 mm for iliac arteries, and from 0.80±0.018 mm to 1.44±0.013 mm for Dacron prostheses). A similar trend, though with a lesser effect, was observed for ring-enforced ePTFE vascular prostheses (from 0.26±0.009 mm to 0.53±0.010 mm). When comparing ring-enforced ePTFE prostheses to iliac arteries, the DD difference was about 76%. Similarly, the DD difference between ring-enforced PTFE and Dacron prostheses was around 71%. In contrast, the difference in DD between iliac arteries and Dacron prostheses was approximately 5%. For the iliac arteries, an increase in EV was associated with a decrease in the magnitude of diameter dilation. When EV increased from 70 ml to 85 ml, the DD difference was approximately 10%, with values of 1.04±0.016 mm for 70 ml and 1.14±0.016 mm for 85 ml. Increasing the EV from 85 ml to 100 ml reduced the *Dd* difference to about 8%, with values of 1.14±0.016 mm for 85 ml and 1.22±0.014 mm for 100 ml. A further increase in EV to 115 ml resulted in a decrease in the *Dd* difference to around 7%, with values of 1.22±0.014 mm for 100 ml and 1.29±0.014 mm for 115 ml (Fig. 1a). It was observed that for ring-enforced ePTFE vascular prostheses, an increase in EV was linked to a nearly constant degree of DD. When the EV increased from 70 ml to 85 ml, the DD difference was about 3%, with measurements of 0.36±0.008 mm for 70 ml and 0.39±0.011 mm for 85 ml. Increasing the EV from 85 ml to 100 ml resulted in a similar 3% difference in *Dd*, with values of 0.39±0.011 mm for 85 ml and 0.42±0.009 mm for 100 ml. A further rise in EV (up to 115 ml) led to a slight increase in the DD difference to approximately 4%, with values of 0.42±0.009 mm for 100 ml and 0.46±0.011 mm for 115 ml (Fig. 1b). Similarly, for Dacron vascular prostheses, an increase in EV was associated with a nearly constant degree of diameter dilation. A change in EV from 70 ml to 85 ml resulted in an 8% difference in diameter DD, with values of 1.00±0.017 mm for 70 ml and 1.08±0.017 mm for 85 ml. Increasing the ejection volume from 85 ml to 100 ml resulted in a similar 8% difference in DD, with values of 1.08±0.017 mm for 85 ml and 1.16±0.015 mm for 100 ml. A further increase in ejection volume to 115 ml led to a slight decrease in the DD difference to around 7%, with values of 1.16±0.015 mm for 100 ml and 1.23±0.011 mm for 115 ml (Fig. 1c).

The experimental results were validated using 2DSTT data, revealing significant differences between the MmCM and 2DSTT outcomes. For the iliac arteries, at an PF of 75 1/min, DD was 0.94±0.012 mm for MmCM and 0.92±0.018 mm for 2DSTT ($p = 0.0273$). At an PF of 90 1/min, DD was 1.04±0.012 mm for MmCM and 1.02±0.015 mm for 2DSTT ($p = 0.009$). A similar trend was observed for ring-enforced ePTFE prostheses: at an PF of 75 1/min, DD was 0.32±0.007 mm for MmCM and 0.30±0.011 mm for 2DSTT ($p = 0.029$), and at 90 1/min, DD was 0.36±0.005 mm for MmCM and 0.34±0.012 mm for 2DSTT ($p = 0.017$). For Dacron prostheses, DD at 75 1/min was 0.89±0.022 mm for MmCM and 0.84±0.027 mm for 2DSTT ($p = 0.004$), and at 90 1/min, *Dd* was 1.00±0.009 mm for MmCM and 0.98±0.009 mm for 2DSTT ($p = 0.001$) (Table 1).

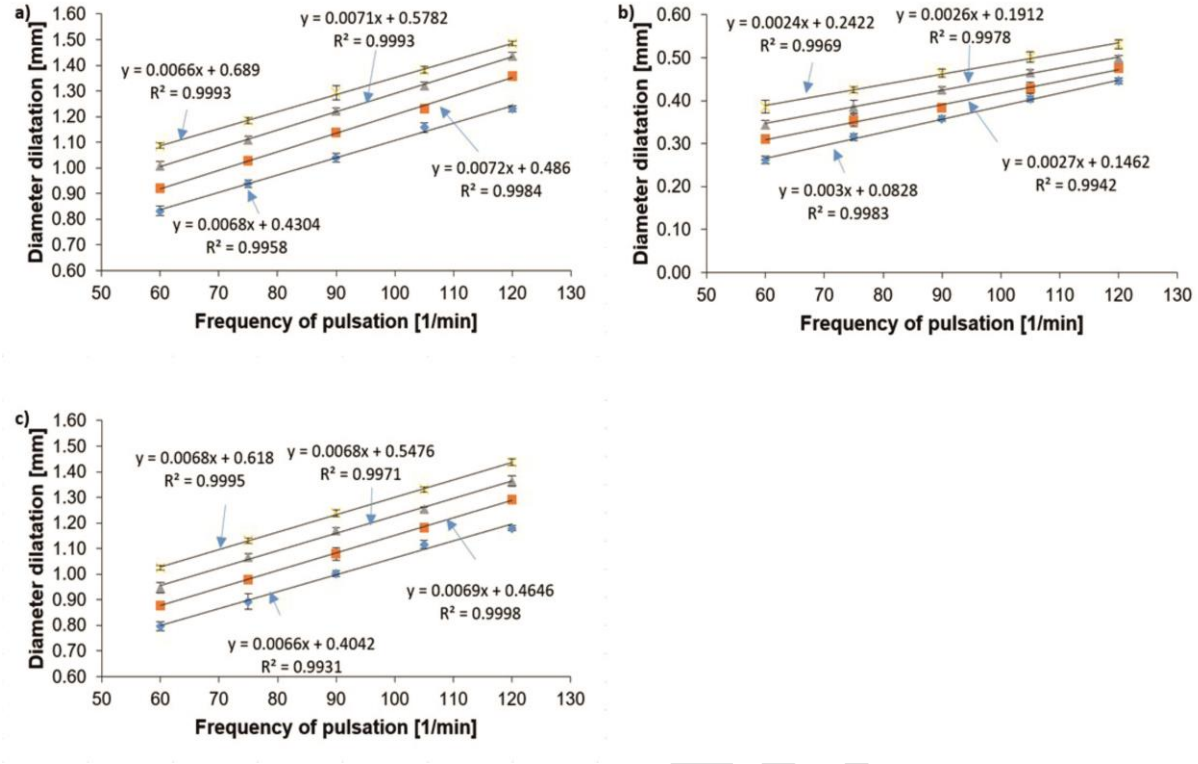

Fig. 1. Diameter dilatation DD [mm] for (a) iliac arteries, (b) ring enforced ePTFE vascular prostheses, (c) Dacron vascular prostheses for ejection volume equal to 70 ml (blue rhombus), 85 ml (orange square), 100 ml (purple triangle), 115 ml (yellow cross).

Table 1. Changes in diameter [mm] for iliac arteries, ring enforced ePTFE and Dacron vascular prostheses. Data are presented as median ($Q1$; $Q2$). $N = 10$, P-values were calculated using T test.

Type of vessel	**Average change of diameter** [mm]		**Median** [mm]		**Low Q** [mm]		**Top Q** [mm]		**P**
	MmCM	2DSTT	MmCM	2DSTT	MmCM	2DSTT	MmCM	2DSTT	
75 [1/min]									
iliac arteries	0.94±0.012	0.92±0.018	0.94	0.92	0.91	0.88	0.96	0.95	0.0273
ePTFE	0.32±0.007	0.30±0.011	0.32	0.30	0.30	0.28	0.33	0.32	0.029
Dacron	0.89±0.022	0.84±0.027	0.91	0.85	0.83	0.79	0.92	0.88	0.004
90 [1/min]									
iliac arteries	1.04±0.012	1.02±0.015	1.04	1.02	1.02	0.99	1.07	1.04	0.009
ePTFE	0.36±0.005	0.34±0.012	0.36	0.34	0.35	0.32	0.37	0.36	0.017
Dacron	1.00±0.009	0.98±0.009	1.00	0.98	0.99	0.96	1.02	1.00	0.001

Additionally, Bland-Altman analysis showed that for the iliac arteries at PF = 75 1/min, the difference between MmCM and 2DSTT was 0.02 mm within a range of 0.06 mm (Fig. 2a), and at PF = 90 1/min, it was 0.03 mm within a range of 0.08 mm (Fig. 2b). For ring-enforced ePTFE prostheses, at PF = 75 1/min, the difference was 0.01 mm within a range of 0.04 mm (Fig. 2c), and at PF = 90 1/min, it was 0.02 mm within a range of 0.06 mm (Fig. 2d). For Dacron prostheses, at PF = 75 1/min, the difference was 0.05 mm within a range of 0.15 mm (Fig. 2e), and at PF = 90 1/min, the difference was 0.02 mm within a range of 0.07 mm (Fig. 2f).

Spearman's rank correlation coefficients were calculated to examine the relationship between DD and hemodynamic parameters (PF and EV). A very strong positive correlation was found between PF and DD. This correlation was significant for the iliac arteries ($rho = 0.853$; $p < 0.0001$), Dacron vascular prostheses ($rho = 0.858$; $p < 0.0001$), and ring-enforced ePTFE

vascular prostheses (*rho* = 0.824; $p < 0.0001$) (Table 3). In contrast, the correlation between EV and DD was moderate. This association was also significant for the iliac arteries (*rho* = 0.499; $p < 0.0001$), Dacron vascular prostheses (*rho* = 0.493; $p < 0.0001$), and ring-enforced ePTFE vascular prostheses (*rho* = 0.535; $p < 0.0001$) (Table 3).

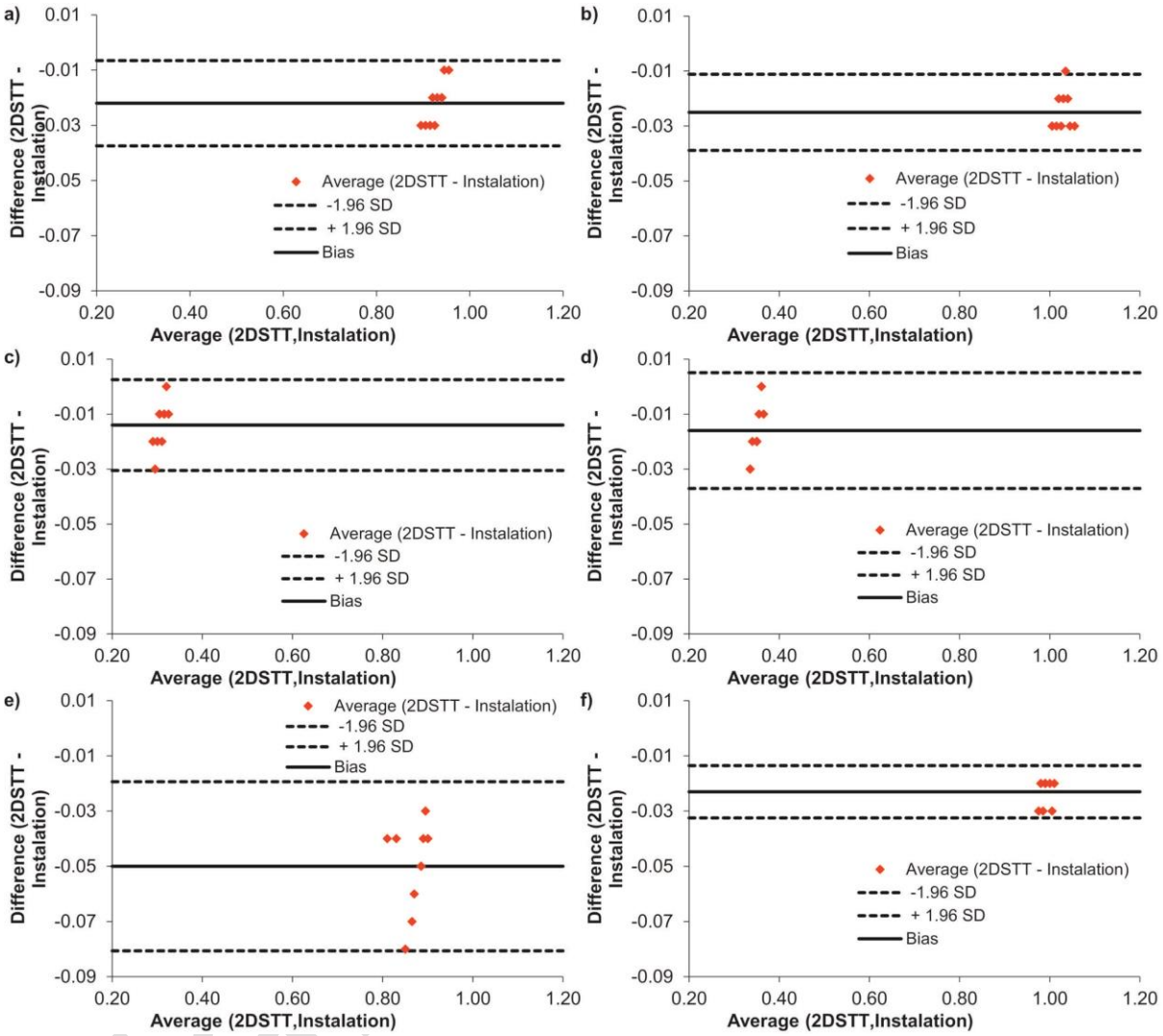

Fig. 2 Comparison of MmCM and 2DSTT for the iliac arteries, ring enforced ePTFE and Dacron vascular prostheses with the use of Bland-Altman analysis for: a) iliac arteries MmCM vs. 2DSTT for PF = 75 1/min, b) iliac arteries MmCM vs. 2DSTT for PF = 90 1/min, c) ring enforced ePTFE vascular prostheses MmCM vs. 2DSTT for PF = 75 1/min, d) ring enforced ePTFE vascular prostheses MmCM vs. 2DSTT for PF = 90 1/min, e) Dacron vascular prostheses MmCM vs. 2DSTT for PF = 75 1/min, f) Dacron vascular prostheses MmCM vs. 2DSTT for PF = 90 1/min.

Additionally, it was observed that at a pulsation frequency of 60 1/min and an ejection volume of 70 ml, the diameter dilation was 0.57 mm greater in iliac arteries compared to ring-enforced ePTFE vascular prostheses, but only 0.04 mm higher compared to Dacron vascular prostheses. Increasing the pulsation frequency from 75 1/min to 120 1/min resulted in a 0.62 mm, 0.68 mm, 0.75 mm, and 0.78 mm increase in the diameter dilation difference between iliac arteries and ring-enforced ePTFE vascular prostheses, respectively. In contrast, for Dacron vascular prostheses, increasing the pulsation frequency resulted in a much smaller increase in the diameter dilation difference with values of 0.05 mm, 0.04 mm, 0.04 mm, and 0.05 mm for the respective frequencies of 75 1/min, 90 1/min, 105 1/min, and 120 1/min. Furthermore, comparing the ring-enforced ePTFE vascular prostheses to Dacron vascular

prostheses, increasing the pulsation frequency from 60 1/min to 120 1/min led to a rise in the diameter dilation difference for Dacron prostheses, with increases of 0.53 mm, 0.58 mm, 0.64 mm, 0.71 mm, and 0.73 mm at 60 1/min, 75 1/min, 90 1/min, 105 1/min, and 120 1/min, respectively (Fig. 3a).

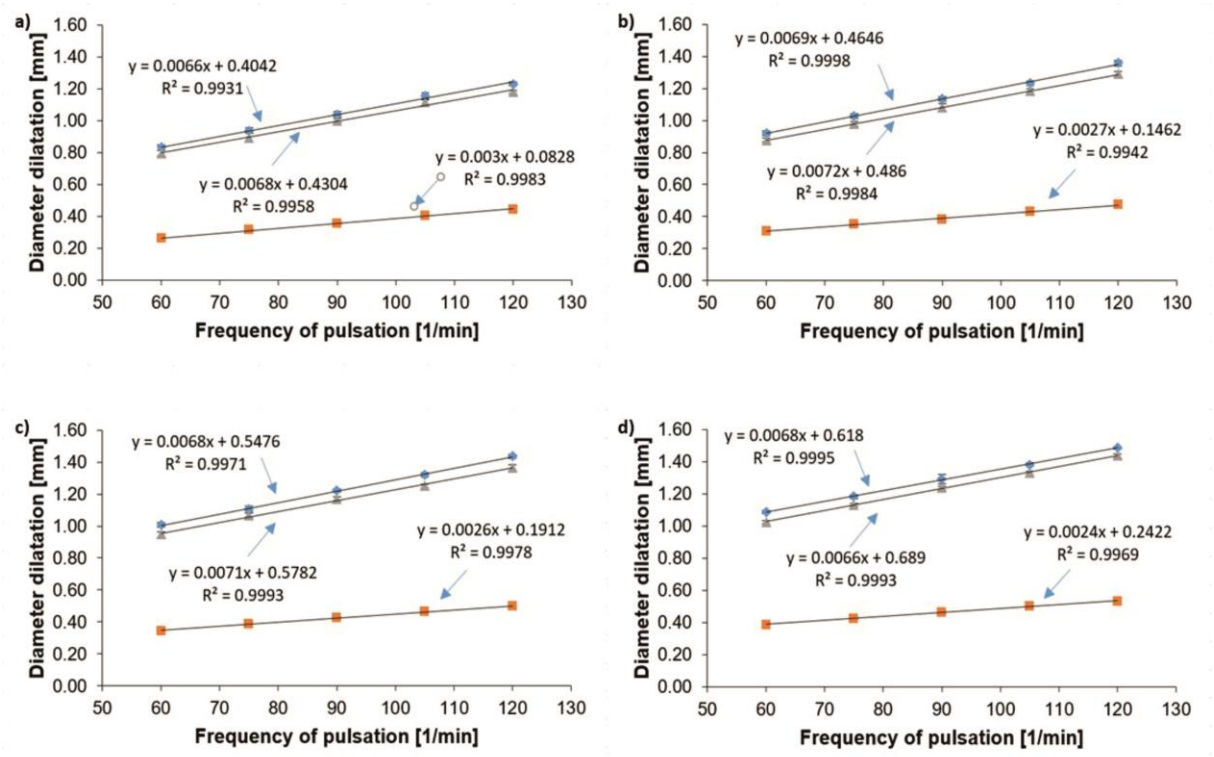

Fig. 3. Comparison of diameter dilatation for ejection volume equal to (a) 70 ml, (b) 85 ml, (c) 100 ml, (d) 115 ml for the iliac arteries (blue rhombus), ring enforced ePTFE vascular prostheses (orange square) and Dacron vascular prostheses (purple triangle).

At a pulsation frequency of 60 1/min and an ejection volume of 85 ml, the diameter dilation was 0.61 mm greater in iliac arteries compared to ring-enforced ePTFE vascular prostheses, but only 0.04 mm greater compared to Dacron vascular prostheses. Increasing the pulsation frequency from 75 1/min to 120 1/min resulted in a 0.67 mm, 0.75 mm, 0.80 mm, and 0.88 mm increase in the diameter dilation difference between iliac arteries and ring-enforced ePTFE prostheses, respectively. In contrast, for Dacron prostheses, increasing the pulsation frequency led to smaller increases of 0.05 mm, 0.06 mm, 0.05 mm, and 0.07 mm in the diameter dilation difference between iliac arteries and Dacron prostheses, respectively. When comparing ring-enforced ePTFE prostheses to Dacron prostheses, increasing the pulsation frequency from 60 1/min to 120 1/min resulted in an increase in the diameter dilation difference for Dacron prostheses, with values of 0.57 mm, 0.63 mm, 0.70 mm, 0.75 mm, and 0.82 mm for 60 1/min, 75 1/min, 90 1/min, 105 1/min, and 120 1/min, respectively (Fig. 3b). For a pulsation frequency of 60 1/min and an ejection volume of 100 ml, the diameter dilation was 0.66 mm higher for iliac arteries compared to the ring-enforced ePTFE vascular prostheses, but only 0.06 mm higher compared to the Dacron vascular prostheses. Furthermore, increasing the pulsation frequency from 75 1/min to 120 1/min (for 75 1/min, 90 1/min, 105 1/min, and 120 1/min) resulted in a 0.72 mm, 0.80 mm, 0.85 mm, and 0.94 mm increase in the diameter dilation difference between iliac arteries and ring-enforced ePTFE vascular prostheses, respectively. In contrast, increasing the pulsation frequency for Dacron vascular prostheses resulted in a 0.04 mm, 0.05 mm, 0.07 mm, and 0.07 mm increase in the diameter dilation difference

between iliac arteries and Dacron vascular prostheses, respectively. However, a comparison of ring-enforced ePTFE vascular prostheses with Dacron vascular prostheses indicated that increasing the pulsation frequency from 60 1/min to 120 1/min (for 60 1/min, 75 1/min, 90 1/min, 105 1/min, and 120 1/min) provoked an increase in the diameter dilation difference for Dacron vascular prostheses (by 0.60 mm, 0.68 mm, 0.74 mm, 0.79 mm, and 0.87 mm, respectively) (Fig. 3c). For a pulsation frequency of 60 1/min and an ejection volume of 100 ml, the diameter dilation was 0.66 mm greater for iliac arteries compared to ring-enforced ePTFE vascular prostheses, but only 0.06 mm greater compared to Dacron vascular prostheses. Increasing the pulsation frequency from 75 1/min to 120 1/min resulted in a 0.72 mm, 0.80 mm, 0.85 mm, and 0.94 mm increase in the diameter dilation difference between iliac arteries and ring-enforced ePTFE prostheses, respectively. For Dacron vascular prostheses, increasing the pulsation frequency resulted in smaller increases of 0.04 mm, 0.05 mm, 0.07 mm, and 0.07 mm in the diameter dilation difference between iliac arteries and Dacron prostheses, respectively. Finally, comparing the ring-enforced ePTFE prostheses with Dacron prostheses showed that increasing the pulsation frequency from 60 1/min to 120 1/min provoked a larger increase in the diameter dilation difference for Dacron prostheses (by 0.60 mm, 0.68 mm, 0.74 mm, 0.79 mm, and 0.87 mm, respectively) (Fig. 3d).

3.2. Wall displacement

The next parameter analyzed was *WD*. It was found that the highest *WD* occurred in the Dacron vascular prostheses, ranging from 7.48±0.170 mm to 12.58±0.096 mm (Fig. 4c). A similar trend was observed for the iliac arteries, though the WD was approximately 25% lower, ranging from 5.80±0.043 mm to 10.30±0.089 mm (Fig. 4a). Similarly, the ring-enforced ePTFE vascular prostheses exhibited behavior similar to the Dacron prostheses, but with values approximately 10% lower, ranging from 4.84±0.029 mm to 8.06±0.030 mm (Fig. 4b).

At a pulsation frequency of 60 1/min and an ejection volume of 70 ml, the wall displacement in the iliac arteries was 0.014 mm higher than in the ring-enforced ePTFE prostheses, but 0.126 mm higher than in the Dacron prostheses. Increasing the pulsation frequency from 75 1/min to 120 1/min (for 75 1/min, 90 1/min, 105 1/min, and 120 1/min) caused the diameter dilation difference between iliac arteries and ring-enforced ePTFE prostheses to increase by 0.003 mm, 0.005 mm, 0.007 mm, and 0.001 mm, respectively. Conversely, for the Dacron prostheses, the dilation difference increased by 0.259 mm, 0.013 mm, 0.022 mm, and 0.000 mm, respectively. When comparing the ring-enforced ePTFE prostheses to Dacron prostheses, the increase in pulsation frequency from 60 1/min to 120 1/min caused the diameter dilation difference to rise for the Dacron prostheses by 0.141 mm, 0.256 mm, 0.008 mm, 0.029 mm, and 0.000 mm, respectively (Fig. 5a).

For a pulsation frequency of 60 1/min and an ejection volume of 85 ml, the wall displacement in the iliac arteries was 0.023 mm higher than in the ring-enforced ePTFE prostheses, but 0.029 mm higher compared to the Dacron prostheses. Increasing the pulsation frequency from 75 1/min to 120 1/min caused the diameter dilation difference between the iliac arteries and ring-enforced ePTFE prostheses to increase by 0.075 mm, 0.002 mm, 0.008 mm, and 0.0048 mm, respectively. For the Dacron prostheses, the increase was 0.064 mm, 0.091 mm, 0.050 mm, and 0.054 mm, respectively. In comparing the two prostheses, the increase in pulsation frequency from 60 1/min to 120 1/min caused the diameter dilation difference for Dacron prostheses to rise by 0.006 mm, 0.012 mm, 0.093 mm, 0.058 mm, and 0.007 mm, respectively (Fig. 5b). For a pulsation frequency of 60 1/min and an ejection volume of 100 ml, the wall displacement in the iliac arteries was 0.010 mm higher compared to the ring-enforced ePTFE prostheses, but 0.005 mm higher compared to the Dacron prostheses. Increasing the pulsation frequency from 75 1/min to 120 1/min resulted in the diameter dilation

difference between iliac arteries and ring-enforced ePTFE prostheses increasing by 0.000 mm, 0.008 mm, 0.004 mm, and 0.017 mm, respectively. For the Dacron prostheses, the increase was 0.020 mm, 0.001 mm, 0.021 mm, and 0.013 mm, respectively. When comparing the two prostheses, the diameter dilation difference for Dacron prostheses increased by 0.005 mm, 0.020 mm, 0.009 mm, 0.025 mm, and 0.004 mm, respectively, with the increase in pulsation frequency from 60 1/min to 120 1/min (Fig. 5c).

At a pulsation frequency of 60 1/min and an ejection volume of 115 ml, the wall displacement was 0.002 mm higher in the iliac arteries compared to the ring-enforced ePTFE vascular prostheses, and 0.004 mm higher compared to the Dacron vascular prostheses. Additionally, increasing the pulsation frequency from 75 1/min to 120 1/min (for 75 1/min, 90 1/min, 105 1/min, and 120 1/min) resulted in a 0.015 mm, 0.002 mm, 0.004 mm, and 0.042 mm increase in the diameter dilation difference between the iliac arteries and the ring-enforced ePTFE vascular prostheses, respectively. In contrast, for the Dacron vascular prostheses, the increase in diameter dilation difference was 0.034 mm, 0.002 mm, 0.009 mm, and 0.023 mm, respectively. When comparing the ring-enforced ePTFE vascular prostheses with the Dacron prostheses, increasing the pulsation frequency from 60 1/min to 120 1/min (for 60 1/min, 75 1/min, 90 1/min, 105 1/min, and 120 1/min) caused the diameter dilation difference to increase for the Dacron prostheses by 0.003 mm, 0.018 mm, 0.001 mm, 0.004 mm, and 0.066 mm, respectively (Fig. 5d).

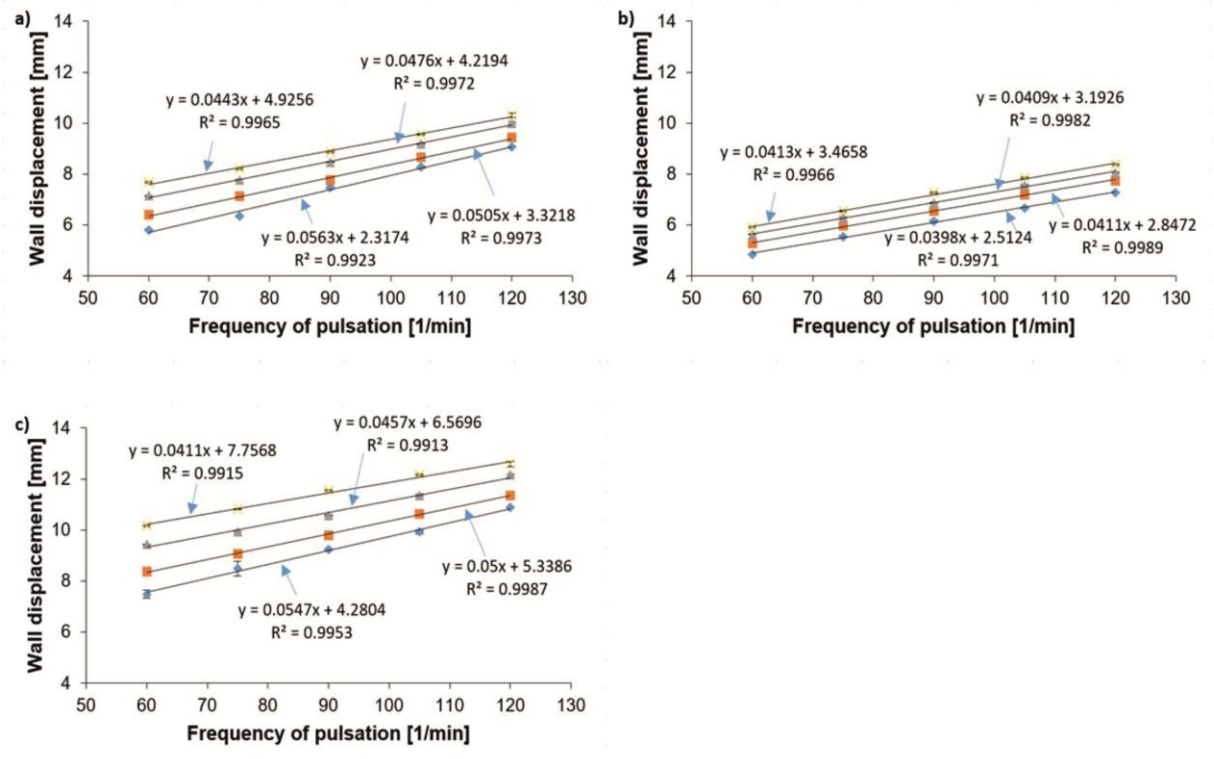

Fig. 4. WD [mm] for (a) iliac arteries, (b) ring enforced ePTFE vascular prostheses, (c) Dacron vascular prostheses for ejection volume equal to 70 ml (blue rhombus), 85 ml (orange square), 100 ml (purple triangle), 115 ml (yellow cross).

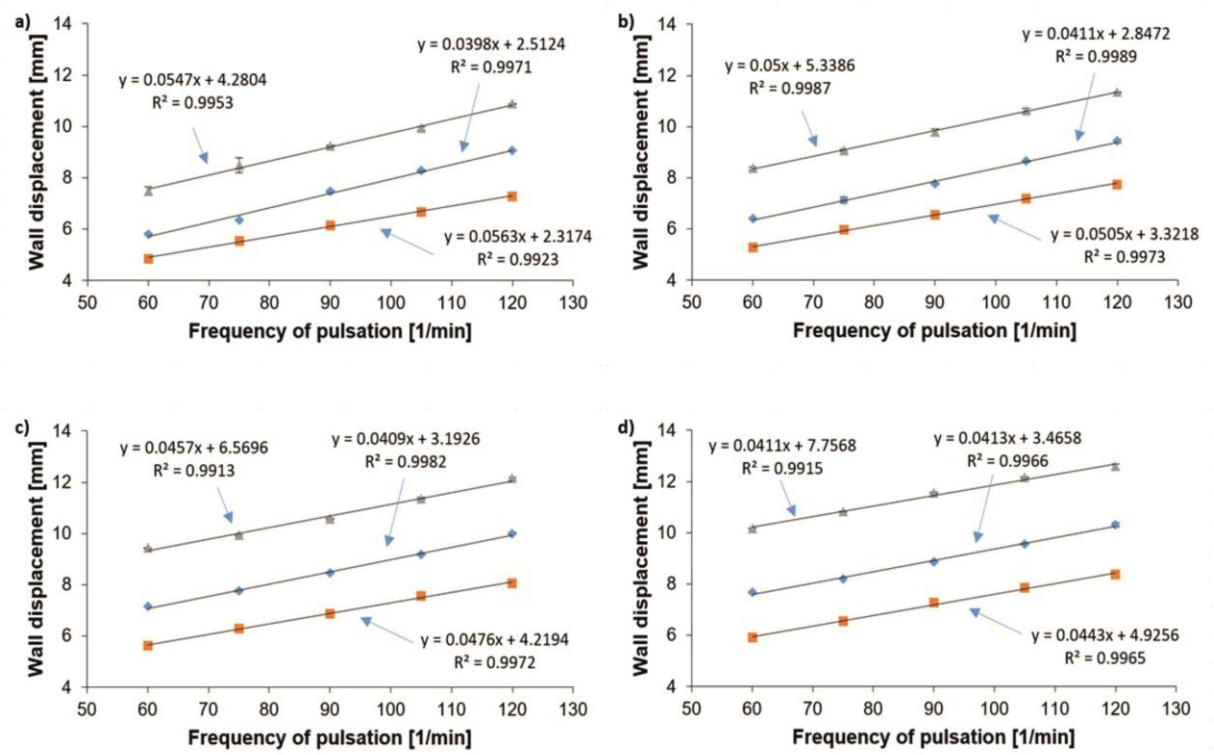

Fig. 5. Comparison of WD for ejection volume equal to (a) 70 ml, (b) 85 ml, (c) 100 ml, (d) 115 ml for the iliac arteries (blue rhombus), ring enforced ePTFE vascular prostheses (orange square) and Dacron vascular prostheses (purple triangle).

4. Discussion

In our previous studies, we demonstrated the capability of an *ex vivo* bioreactor to replicate hemodynamic in elastic 3D-printed models of abdominal aortic aneurysms [29] and human grafts [12, 28, 31]. These studies demonstrated the ability of our custom-built system to effectively monitor hemodynamic changes in abdominal aortic aneurysm models under varying hemodynamic conditions, regardless of the presence of thrombus or a stent-graft. We aimed to assess the accuracy of our platform in simulating the movement of synthetic vascular prostheses in comparison to iliac arteries under fluctuating cardiovascular parameters, such as heartbeat and ejection fraction. To the best of our knowledge, our MmCM is the first artificial model capable of analyzing these factors, as current vascular bioreactors do not monitor the mechanical properties of the vessels being studied. Additionally, there is no existing data on the use of vision systems for 3D projection of vessel wall behavior after placement in bioengineering reactors. It should be mentioned that systems have been developed, such as the *ex vivo* vessel culture system to replicate hemodynamic factors in the coronary circulation. However, the impact of altered flow conditions has only been studied in human saphenous veins following coronary artery bypass grafting [32].

Vascular replacement and repair for treating atherosclerotic disease, infections, and traumatic injuries are among the most frequently performed surgical procedures in the Western world [33]. Therefore, 3D printing offers several benefits in terms of biocompatibility. It allows the precise customization of medical implants and tissue scaffolds, tailored to meet individual patient needs and accommodate complex anatomical structures [34]. Different techniques are adopted for artificial blood vessels production [35]. *Stereolithography* (SLA) is a prominent 3D printing technique for creating intricate artificial blood vessels. It has been observed that SLA bioprinting's ability to produce smooth surfaces helps replicate the natural environment of blood

vessels [36, 37]. *Selective laser sintering* (SLS) bioprinting technique is a key one among the 3D printing methods employed to create complex artificial blood vessels. Authors observed that the strength of SLS lies in its versatility with materials, allowing the use of various biomaterials, as well as its ability to fabricate complex geometries [38, 39]. The correlation observed in our study between the mechanical properties of PTFE and Dacron vessels and iliac arteries is consistent with the enhanced mechanical properties reported by Wang *et al.* for synthetic non-biodegradable materials such as PET, ePTFE, and PU [32].

It is very common to reconstruct blood flow using artificial and real vessels, but within the human body, rather than with artificial systems [40, 41]. This allows the reconstruction of blood flow, but only according to the hemodynamic of the specific patient. For this reason, we developed our own device that enables the reconstruction of any blood flow parameters. In the future, the MmCM introduced in this study have applications in a wide range of vascular issues. Primarily, it can provide detailed insights into new vascular grafts, as well as those already in clinical use.

The limitation of the study primarily focuses on the spatial configuration of the Man-made Circulatory Model. The iliac arteries, ring-enforced ePTFE vascular prostheses, and Dacron vascular prostheses were restricted to a length of 100 mm due to the chamber's dimensions. This limitation is dictated by the geometry of the MmCM. To improve the model's flexibility, future iterations should consider modifications to accommodate vessels of both shorter and longer lengths. Additionally, the inlet and outlet pipes were designed for vessels within the size range of the iliac arteries, limiting their compatibility with smaller vessels. To expand the MmCM's applicability, further adjustments are needed to accommodate smaller vessels.

5. Conclusions

DD in vascular prostheses is influenced by EV and PF, with iliac arteries and Dacron prostheses showing higher DD than ring-enforced ePTFE prostheses. Increasing EV and PF results in greater DD, especially in iliac arteries and Dacron prostheses. DD correlates strongly with PF and moderately with EV. Pulsation frequency also affects dilation, with iliac arteries showing the greatest dilation and Dacron the least.

Validation through MmCM and 2DSTT models shows consistent trends in DD, indicating that pulsation frequency and ejection volume are key factors in prosthesis performance, aiding clinical prosthesis selection.

WD is affected by material type and pulsation frequency, with Dacron prostheses showing higher displacement than ring-enforced ePTFE, and iliac arteries having intermediate values. As pulsation frequency increases, dilation differences between iliac arteries and prostheses grow, revealing varying mechanical behaviors. These insights inform the design of improved vascular grafts with better patency.

Acknowledgements

The study was approved by the local Institutional Review Board (2069/2012) of the Medical University of Vienna. The study was supported by the Polish National Centre for Research and Development (501/10-34-19-605 to AP) and by grant number 181110 from the Medical University of Vienna, Department of Surgery, Division of Vascular Surgery (to IH). In the following study, BRaIn Laboratories of the Medical University of Lodz in the field of hemodynamic were used.

References

[1] Vaduganathan, M., Mensah, G. A., Turco, J. V., Fuster, V., & Roth, G. A. (2022). The global burden of cardiovascular diseases and risk: a compass for future health. *Journal of the American College of Cardiology*, *80* (25), 2361–2371. https://doi.org/10.1016/j.jacc.2022.11.005

[2] Polanczyk, A., Piechota-Polanczyk, A., Piastowska-Ciesielska, A. W., Huk, I., Neumayer, C., Wadowski, P. P., Balcer, J., & Strzelecki, M. (2024). Computational fluid dynamic as an engineering tool for the reconstruction of blood hemodynamics and spatial configuration before and after endoleak appearance. *Metrology and Measurement Systems*, 711. https://doi.org/10.24425/mms.2024.152053

[3] Martin, S. S., *et al.*Aday, A. W., Almarzooq, Z. I., Anderson, C. A., Arora, P., Avery, C. L., Baker-Smith, C. M., Gibbs, B. B., Beaton, A. Z., Boehme, A. K., Commodore-Mensah, Y., Currie, M. E., Elkind, M. S., Evenson, K. R., Generoso, G., Heard, D. G., Hiremath, S., Johansen, M. C., Kalani, R., & Palaniappan, L. P. (2024). 2024 Heart Disease and stroke statistics: A report of US and global data from the American Heart Association. *Circulation*, *149* (8). https://doi.org/10.1161/cir.0000000000001209

[4] Kapuku, G. K., & Kop, W. J. (2022). Classification of Cardiovascular Diseases: Epidemiology, diagnosis, and treatment. In *Springer eBooks* (pp. 45–80). https://doi.org/10.1007/978-0-387-85960-6_3

[5] Polanczyk, A., Piechota-Polanczyk, A., Huk, I., Neumayer, C., Balcer, J., & Strzelecki, M. (2021). Computational fluid dynamic technique for assessment of how changing character of blood flow and different value of HCT influence blood hemodynamic in dissected aorta. *Diagnostics*, *11* (10), 1866. https://doi.org/10.3390/diagnostics11101866

[6] Piché, M., Tchernof, A., & Després, J. (2020). Obesity phenotypes, diabetes, and cardiovascular diseases. *Circulation Research*, *126* (11), 1477–1500. https://doi.org/10.1161/circresaha.120.316101

[7] Polanczyk, A., Piechota-Polanczyk, A., Stefańczyk, L., & Strzelecki, M. (2020). Spatial configuration of abdominal aortic aneurysm analysis as a useful tool for the estimation of Stent-Graft migration. *Diagnostics*, *10* (10), 737. https://doi.org/10.3390/diagnostics10100737

[8] Boukhennoufa, N., Laamari, Y., & Benzid, R. (2024). Signal denoising using a low computational translationin-variant- like strategy involving multiple wavelet bases: application to synthetic and ECG signals. *Metrology and Measurement Systems*, 31 (2), 259–278. https://doi.org/10.24425/mms.2024.148548

[9] Sadr, H., Salari, A., Ashoobi, M. T., & Nazari, M. (2024). Cardiovascular disease diagnosis: a holistic approach using the integration of machine learning and deep learning models. *European Journal of Medical Research*, *29* (1). https://doi.org/10.1186/s40001-024-02044-7

[10] Polanczyk, A., Piechota-Polanczyk, A., & Stefańczyk, L. (2017). A new approach for the pre-clinical optimization of a spatial configuration of bifurcated endovascular prosthesis placed in abdominal aortic aneurysms. *PLoS ONE*, *12* (8), e0182717. https://doi.org/10.1371/journal.pone.0182717

[11] Duong, W., Grigorian, A., Yuen, S., Nahmias, n.-K., Kabutey, N., Farzaneh, C., Donayre, C., & Fujitani, R. M. (2023). Increased mortality in octogenarians undergoing endovascular aortic aneurysm repair for smaller aneurysms warrants caution. *Annals of Vascular Surgery*, *99*, 175–185. https://doi.org/10.1016/j.avsg.2023.07.107

[12] Polanczyk, A., Piechota-Polanczyk, A., Piastowska-Ciesielska, A. W., Huk, I., Neumayer, C., Balcer, J., & Strzelecki, M. (2024). Reconstruction of the physiological behavior of real and synthetic vessels in controlled conditions. *Applied Sciences*, *14* (6), 2600. https://doi.org/10.3390/app14062600

[13] Moise, K., Arun, K. M., Pillai, M., Salvador, J., Mehta, A. S., Goyal, Y., & Iruela-Arispe, M. L. (2024). Endothelial cell elongation and alignment in response to shear stress requires acetylation of microtubules. *Frontiers in Physiology*, *15*. https://doi.org/10.3389/fphys.2024.1425620

[14] Carvalho, V., Gonçalves, I. M., Souza, A., Souza, M. S., Bento, D., Ribeiro, J. E., Lima, R., & Pinho, D. (2021). Manual and automatic image analysis segmentation methods for blood flow studies in microchannels. *Micromachines*, *12* (3), 317. https://doi.org/10.3390/mi12030317

[15] Luijten, B., Chennakeshava, N., Eldar, Y. C., Mischi, M., & Van Sloun, R. J. (2023). Ultrasound Signal processing: From models to deep learning. *Ultrasound in Medicine & Biology*, *49* (3), 677–698. https://doi.org/10.1016/j.ultrasmedbio.2022.11.003

[16] Le, T. M., Paul, J. S., Al-Nashash, H., Tan, A., Luft, A. R., Sheu, F. S., & Ong, S. H. (2007). New Insights into Image Processing of Cortical Blood Flow Monitors Using Laser Speckle Imaging. *IEEE Transactions on Medical Imaging*, *26* (6), 833–842. https://doi.org/10.1109/tmi.2007.892643

[17] Dumitrascu, O. M., & Qureshi, T. A. (2018). Retinal Vascular Imaging in Vascular Cognitive Impairment: Current and future Perspectives. *Journal of Experimental Neuroscience*, *12*. https://doi.org/10.1177/1179069518801291

[18] Du, C., Zhuang, J., & Huang, X. (2024). Deep learning technology in vascular image segmentation and disease diagnosis. *Journal of Intelligent Medicine.* https://doi.org/10.1002/jim4.15

[19] Abdulsahib, A. A., Mahmoud, M. A., Aris, H., Gunasekaran, S. S., & Mohammed, M. A. (2022). An automated image segmentation and useful feature extraction algorithm for retinal blood vessels in Fundus images. *Electronics*, *11*(9), 1295. https://doi.org/10.3390/electronics11091295

[20] Czepita, M., & Fabijańska, A. (2021). Image processing pipeline for the detection of blood flow through retinal vessels with subpixel accuracy in fundus images. *Computer Methods and Programs in Biomedicine*, *208*, 106240. https://doi.org/10.1016/j.cmpb.2021.106240

[21] Khan, B., Riaz, Z., Ahmad, R. U. S., & Khoo, B. L. (2024). Advancements in wearable sensors for cardiovascular disease detection for health monitoring. *Materials Science and Engineering R Reports*, *159*, 100804. https://doi.org/10.1016/j.mser.2024.100804

[22] Chrzanowski, L., Drozdz, J., Strzelecki, M., Krzeminska-Pakula, M., Jedrzejewski, K. S., & Kasprzak, J. D. (2007). Application of neural networks for the analysis of intravascular ultrasound and histological Aortic Wall Appearance—An In Vitro Tissue Characterization study. *Ultrasound in Medicine & Biology*, *34*(1), 103–113. https://doi.org/10.1016/j.ultrasmedbio.2007.06.021

[23] Szmajda, M., Chyliński, M., Szacha, J., & Mroczka, J. (2023). Three methods for determining respiratory waves from ECG (Part I). *Metrology and Measurement Systems*, 30 (4), 821–837. https://doi.org/10.24425/mms.2023.147956

[24] DeGroat, W., Abdelhalim, H., Patel, K., Mendhe, D., Zeeshan, S., & Ahmed, Z. (2024). Discovering biomarkers associated and predicting cardiovascular disease with high accuracy using a novel nexus of machine learning techniques for precision medicine. *Scientific Reports*, *14* (1). https://doi.org/10.1038/s41598-023-50600-8

[25] Mirani, B., Latifi, N., Lecce, M., Zhang, X., & Simmons, C. A. (2024). Biomaterials and biofabrication strategies for tissue-engineered heart valves. *Matter*, *7* (9), 2896–2940. https://doi.org/10.1016/j.matt.2024.05.036

[26] Piola, M., Prandi, F., Bono, N., Soncini, M., Penza, E., Agrifoglio, M., Polvani, G., Pesce, M., & Fiore, G. B. (2013). A compact and automatedex vivovessel culture system for the pulsatile pressure conditioning of human saphenous veins. *Journal of Tissue Engineering and Regenerative Medicine*, *10* (3), E204–E215. https://doi.org/10.1002/term.1798

[27] Garoffolo, G., Ruiter, M. S., Piola, M., Brioschi, M., Thomas, A. C., Agrifoglio, M., Polvani, G., Coppadoro, L., Zoli, S., Saccu, C., Spinetti, G., Banfi, C., Fiore, G. B., Madeddu, P., Soncini, M., & Pesce, M. (2020). Coronary artery mechanics induces human saphenous vein remodelling via recruitment of adventitial myofibroblast-like cells mediated by Thrombospondin-1. *Theranostics*, *10* (6), 2597–2611. https://doi.org/10.7150/thno.40595

[28] Polanczyk, A., Klinger, M., Nanobachvili, J., Huk, I., & Neumayer, C. (2018). Artificial circulatory model for analysis of human and artificial vessels. *Applied Sciences*, *8* (7), 1017. https://doi.org/10.3390/app8071017

[29] Polanczyk, A., Podgorski, M., Polanczyk, M., Piechota-Polanczyk, A., Neumayer, C., & Stefanczyk, L. (2018). A novel Patient-Specific Human Cardiovascular System Phantom (HCSP) for reconstructions of pulsatile blood hemodynamic inside abdominal aortic aneurysm. *IEEE Access*, *6*, 61896–61903. https://doi.org/10.1109/access.2018.2876377

[30] Polanczyk, A., Piechota-Polanczyk, A., Neumayer, C., & Huk, I. (2019). CFD Reconstruction of Blood Hemodynamic Based on a Self-made Algorithm in Patients with Acute Type IIIb Aortic Dissection Treated with TEVAR Procedure. In *IUTAM bookseries* (pp. 75–84). https://doi.org/10.1007/978-3-030-13720-5_7

[31] Polanczyk, A., Podgorski, M., Polanczyk, M., Piechota-Polanczyk, A., Stefanczyk, L., & Strzelecki, M. (2019). A novel vision-based system for quantitative analysis of abdominal aortic aneurysm deformation. *BioMedical Engineering OnLine*, *18*(1). https://doi.org/10.1186/s12938-019-0681-y

[32] Wang, G.-L., Xiao, Y., Voorhees, A., Qi, Y.-X., Jiang, Z.-L., & Han, H.-C. (2014). Artery remodeling under axial twist in three days organ culture. *Annals of Biomedical Engineering*, *43* (8), 1738–1747. https://doi.org/10.1007/s10439-014-1215-1

[33] Niklason, L. E., & Lawson, J. H. (2020). Bioengineered human blood vessels. *Science*, *370* (6513). https://doi.org/10.1126/science.aaw8682

[34] Choi, J., Lee, E. J., Jang, W. B., & Kwon, S.-M. (2023). Development of Biocompatible 3D-Printed Artificial Blood Vessels through Multidimensional Approaches. *Journal of Functional Biomaterials*, *14* (10), 497. https://doi.org/10.3390/jfb14100497

[35] Mironov, V., Reis, N., & Derby, B. (2006). Review: Bioprinting: a Beginning. *Tissue Engineering*, *12* (4), 631–634. https://doi.org/10.1089/ten.2006.12.631

[36] Vaz, V.M., & Kumar, L. (2021). 3D printing as a promising tool in personalized medicine. *AAPS PharmSciTech*, *22* (1). https://doi.org/10.1208/s12249-020-01905-8

[37] Deshmane, S., Kendre, P., Mahajan, H., & Jain, S. (2021). Stereolithography 3D printing technology in pharmaceuticals: a review. *Drug Development and Industrial Pharmacy*, *47* (9), 1362–1372. https://doi.org/10.1080/03639045.2021.1994990

[38] Yang, J., Li, H., Xu, L., & Wang, Y. (2021). Selective laser sintering versus conventional lost-wax casting for single metal copings: A systematic review and meta-analysis. *Journal of Prosthetic Dentistry*, *128*(5), 897–904. https://doi.org/10.1016/j.prosdent.2021.02.011

[39] Charoo, N.A., Ali, S.F.B., Mohamed, E.M., Kuttolamadom, M.A., Ozkan, T., Khan, M.A., & Rahman, Z. (2020). Selective laser sintering 3D printing – an overview of the technology and pharmaceutical applications. *Drug Development and Industrial Pharmacy*, *46* (6), 869–877. https://doi.org/10.1080/03639045.2020.1764027

[40] Zhang, Z., Huang, M., & Pan, X. (2020). Prosthetic reconstruction of superior vena cava system for thymic tumor: A retrospective analysis of 22 cases. *The Thoracic and Cardiovascular Surgeon*, *69* (02), 165–172. https://doi.org/10.1055/s-0039-3401044

[41] Wang, X.-Y., Pei, Y., Xie, M., Jin, Z.-H., Xiao, Y.-S., Wang, Y., Zhang, L.-N., Li, Y., & Huang, W.-H. (2014). An artificial blood vessel implanted three-dimensional microsystem for modeling transvascular migration of tumor cells. *Lab on a Chip*, *15* (4), 1178–1187. https://doi.org/10.1039/c4lc00973h

Andrzej Polanczyk is a researcher at Fire University (Poland). He participated in scientific grants in which he built the installation to simulate the blood flow through the abdominal section of the aorta and computer algorithms for 3d shape of aorta and blood hemodynamic reconstruction. His research areas comprise biomedical, chemical and, environmental engineering.

Aleksandra Piechota-Polanczyk is currently employed at the Medical University of Lodz, Department of Cell Cultures and Genomic Analysis (Poland). Her research interests focus on finding of new anti-oxidative and anti-inflammatory proteins that could be potential markers and/or targets in treatment of cardiovascular and gastrointestinal diseases, as well as the role of Nrf2 and heme oxygenase 1 in cellular adaptation to oxidative stress and inflammatory reactions.

Agnieszka W. Piastowska-Ciesielska is currently employed at the Medical University of Lodz, Department of Cell Cultures and Genomic Analysis (Poland). Her research interests focus on broadly understood xenobiotics that can modulate the functioning of both cancerous and normal cells. Her main research focuses on assessing the impact of mycotoxins (produced by mold fungi) on cancer cells derived from the prostate gland.

Ihor Huk was the Director of Vascular Laboratory and Clinical Professor of Surgery, Director of Vascular Laboratory Dept. of Surgery, MUV Medical School (Austria). He completed his Post-graduate education from University of Chicago, Heidelberg Special Training: American Society in Parenteral and Enteral Nutrition transplant surgery. Since 1984 he performed more than 550 kidney, liver transplantation Vascular Surgery: Clinical, experimental Research (SPACE-Study), (L-arginine study). He is a member of Austrian Society of Surgery Austrian Society of Angiology Austrian Society of Vascular Surgery Ukrainian Academy of High Education Ukrainian Academy of Sciences and Senate - Zaporizhzhia Medical Postgraduate Academy Honoris causa.

Christoph Neumayer is a Head of the Department of Vascular Surgery at the Medical University of Vienna (Austria). His research areas are concentrated on the molecular mechanism of artery diseases and diabetes.

Julia Balcer is currently a student at Lodz University of Technology (Poland). Her research interests focus on processing and analysis of images and data analysis methods.

Patricia Pia Wadowski is employed at the Department of Internal Medicine II, Division of Angiology at the Medical University of Vienna (Austria). Her research interests focus on microcirculation, peripheral arterial and aortic diseases, platelets and thromboinflammation.

Michal Strzelecki is employed at the Institute of Electronics, Lodz University of Technology (Poland). His scientific interests include the processing and analysis of biomedical signals and images, data analysis methods, and artificial intelligence. also works on the development of software aimed at support of medical imaging diagnostics. Within these interests, Prof. Strzelecki conducts extensive cooperation with domestic and foreign medical universities on the construction and development of systems supporting the diagnostic process